Preprint Title Microstructure, transport and galvanomagnetic properties of $Ni_{48}Fe_{12}Cr_{40}$ thin films

Authors Roman Zavornitsyn, Mikhail Milyaev, Larisa Naumova, Irina Maksimova, Anastasia Pavlova, Tatyana Chernyshova, Vyacheslav Proglyado and Vladimir Ustinov

Publication Date 20 Feb. 2026

Article Type Full Research Paper

ORCID® iDs Roman Zavornitsyn - https://orcid.org/0000-0002-0445-083X; Larisa Naumova - https://orcid.org/0000-0001-5463-6790; Irina Maksimova - https://orcid.org/0000-0002-2542-3363; Anastasia Pavlova - https://orcid.org/0000-0002-1260-5707; Vyacheslav Proglyado - https://orcid.org/0000-0003-3760-8696

Microstructure, transport and galvanomagnetic properties of $Ni_{48}Fe_{12}Cr_{40}$ thin films

Roman Zavornitsyn*[1,2], Mikhail Milyaev[1,2], Larisa Naumova[1,2], Irina Maksimova[1], Anastasia Pavlova[1], Tatyana Chernyshova[1], Vyacheslav Proglyado[1], Vladimir Ustinov[1]

Address:

[1]Laboratory of Quantum Nanospintronics, M.N. Mikheev Institute of Metal Physics of Ural Branch of Russian Academy of Sciences, S. Kovalevskoi str., 18, Ekaterinburg 620108, Russia

[2]Department of Magnetism and Magnetic Nanomaterials, The Institute of Natural Sciences and Mathematics, Ural Federal University named after the first President of Russia B.N.Yeltsin, Kuybysheva str., 48, Ekaterinburg 620062, Russia

Email:

Roman Zavornitsyn - zavornitsyn@imp.uran.ru

* Corresponding author

Abstract

The microstructure, transport and galvanometric properties of $Ni_{48}Fe_{12}Cr_{40}$ thin films of various thickness, obtained by magnetron sputtering, were studied in the temperature range of 93 – 293 K. The $Ni_{48}Fe_{12}Cr_{40}$ film with thickness of 5 nm has been found to be X-ray amorphous and exhibits negative temperature coefficient of resistance. The observation of anisotropic magnetoresistance, as well as anomalous and planar Hall

effect, indicates the presence of ferromagnetic ordering in this sample. The increase of the $Ni_{48}Fe_{12}Cr_{40}$ film thickness to 8 nm leads to the crystallization and texture formation, which promotes more uniform distribution of Cr atoms in Ni-Fe matrix and suppression of the long-range ferromagnetic order.

Keywords

NiFeCr alloy; thin films; magnetoresistance; Hall effect; permalloy

Introduction

The Ni-Fe – based alloys (permalloy) are the key material for spintronics and magnetic sensorics [1, 2], due to their unique combination of properties: high magnetic permeability, low coercive force and significant anisotropic magnetoresistance (AMR). However, to solve the new technological problems, such as reduction of the power consumption of memory elements [3], it is necessary to modify both transport and magnetic properties of the material. One of the most effective approaches to solving this problem is the alloying Ni-Fe binary alloys with the transition metals, chromium (Cr) in particular [3, 4].

The introduction of chromium into the permalloy lattice leads to the significant changes in the electronic structure and microstructure of the alloy, the nature of which depends on the concentration of alloying additive and film thickness [4, 5]. According to the phase diagram for Ni-Fe-Cr alloys [6], a bulk sample of $Ni_{48}Fe_{12}Cr_{40}$ composition is characterized by the combined presence of α- and γ –phases, which have body-centered cubic (bcc) and face-centered cubic (fcc) structure, respectively. The preferential formation of α- or γ – phase in films and nanolayers of $Ni_{48}Fe_{12}Cr_{40}$ alloy depends on the film thickness as well as on the substrate material or on the preceding

layer of nanostructure. In the work [5] bcc structure was discovered in the 5 nm thick film. We previously investigated the microstructure of $Ni_{48}Fe_{12}Cr_{40}$ layer in superlattices exhibiting the giant magnetoresistance effect [7]. It has been shown that BCC structure is formed in the 6.5 nm thick layer when sputtered on the oxidized single-crystal silicon; however, when sputtered on the Ta sublayer with the same thickness of $Ni_{48}Fe_{12}Cr_{40}$ layer the fcc structure is formed in it.

The substitution of nickel and iron atoms with chromium atoms, which have a larger atomic radius, causes a distortion of the crystal lattice, manifested in the increase of its parameter and growth of microstresses [8]. The increasing structural disorder leads to the sharp increase in specific resistance and to the change of sign of the temperature coefficient of resistance (TCR) from positive to negative, which is characteristic of highly disordered systems [9-11].

Changes in the electron density of states and microstructure at chromium alloying lead to the suppression of ferromagnetic ordering. Chromium atoms in the permalloy lattice have the magnetic moment oriented antiparallel to those Ni and Fe atoms moments that arise the compensation of total magnetic moment and the decrease of saturation magnetization [3]. It has been shown in [4], that at Cr impurity concentration of 10%, the saturation magnetization of permalloy decreases by 30%. The increase of Cr concentration leads to the monotonous decrease of Curie temperature (T_c). For $(Ni_{80}Fe_{20})_{100-x}Cr_x$(11nm) film obtained by magnetron sputtering, T_c varies within 800 – 250 K in the concentration range $0 \leq x \leq 35\%$ [4]. In [12] it is reported that at high concentration of Cr (> 20 - 30%) the system can undergo the phase transitions to spin glass or paramagnetic state at room temperature, exhibiting complex magnetic behavior.

The use of galvanomagnetic effects, the Hall effect in particular, as a sensitive tool for diagnosing the magnetic phase transformations is of particular interest. Since

the anomalous Hall component is directly proportional to the magnetization, the presence or absence of anomalous contribution makes it possible to track the evolution of magnetic state of the system under conditions where classical magnetometry data can be ambiguous [12]. In addition, the Ni-Fe systems alloying with chromium leads to the change of electron band structure and contribution of various groups of charge carriers. Experimentally it is demonstrated by the change of Hall constant sign. In the Ni-Fe-Cr alloys at the increase of Cr concentration from 12 to 18%, the transition from negative values of ordinary (R_0) and anomalous (R_S) Hall coefficients, characteristic of pure Ni or Ni-Fe, to positive ones was observed [2, 13].

The effect of low concentrations of Cr alloying additives on the electrical and magnetic properties of Ni-Fe has been studied in sufficient details. However, the behavior of heavily alloyed alloys remains a subject of debate. For Ni-Fe-Cr system, the critical Cr concentration suppressing the long-range magnetic order is approximately 35-45% [4]. At such concentrations of the alloying element, the alloy presents a highly disordered system. The study of transport and magnetic properties of ultrathin layers (<10 nm) of heavily alloyed Ni-Fe-Cr alloys, which are the functional materials for the modern spintronic devices, is of special interest. In particular, the use of $Ni_{48}Fe_{12}Cr_{40}$ alloy as a buffer layer [5, 7, 14, 15] in the synthesis of magnetic nanostructures leads to the increase of magnetoresistance and decrease of hysteresis due to the formation of pronounced crystal texture (111) and the increase of grain size.

In this paper, the correlation between the microstructure and galvanomagnetic properties of $Ni_{48}Fe_{12}Cr_{40}$ films has been investigated. Basing on the analysis of measurement results of magnetoresistance, anomalous and planar Hall effect, the conclusion about the magnetic ordering of $Ni_{48}Fe_{12}Cr_{40}$ thin films has been made.

Results and Discussion

Microstructure and morphology of $Ni_{48}Fe_{12}Cr_{40}$ films surface

Fig. 1 shows the results of X-ray reflectometry for films of different thickness. The thickness was estimated from the oscillation period of the reflectometry curves obtained for the films t_{NiFeCr} = 8 and 30 nm. The obtained values t_{NiFeCr} = 7.9 and 30.5 nm are close to the nominal thickness specified during sputtering. For the films of different thickness, approximately equal decrease in the intensity of reflected radiation is observed with the increase of angle 2Θ. Consequently, the films have similar values of surface roughness.

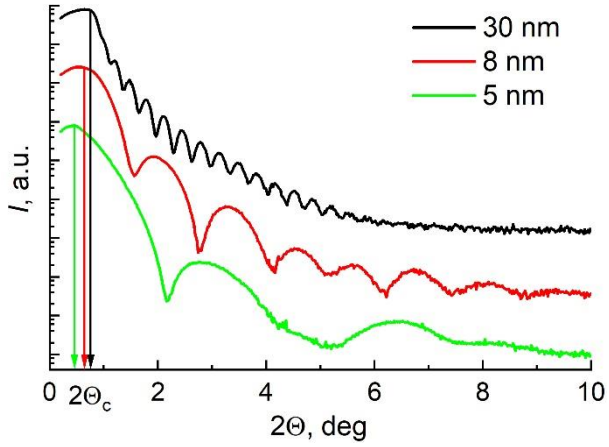

Figure 1: Results of X-ray reflectometry of NiFeCr films with thickness of 5, 8 and 30 nm.

The important characteristic, which can be obtained from the results of X-ray reflectometry is the critical angle ($Θ_c$) of total external reflection of X-rays from the surface of the analyzed film [16, 17]. If the angle between the incident radiation and the sample surface Θ < Θc, the radiation is completely reflected. At Θ > $Θ_c$ the radiation, being refracted, enters the sample and the detector records the decrease in the intensity of reflected signal with the increase of angle 2Θ (Fig. 1). For the films with thickness of 8 and 30 nm the $Θ_c$ values coincide practically, and for the film with 5 nm

thickness the critical angle is noticeably smaller. This difference may be due to the fact, that electron density and, accordingly, the density of the film material at t_{NiFeCr} = 5 nm is less than at t_{NiFeCr} = 8 and 30 nm.

Figure 2 shows the X-ray diffraction patterns obtained for the films of different thickness. For t_{NiFeCr} = 5 nm no diffraction peaks were detected in the entire studied angular range. Basing on the X-ray amorphism of this sample, it can be assumed, that 5nm thick film has a disordered fine-crystalline microstructure. With the increase of the film thickness the reflections (111) and (222), corresponding to the fcc lattice, appear in the diffraction pattern. Texture investigations have shown, that the width at half-height of the rocking curve (ω-scan) around the (111) peak is 9 and 11 degrees for films with thickness of 8 and 30 nm, respectively. Therefore, for t_{NiFeCr} = 8 and 30 nm the axial texture <111> is formed, and the average angle of texture axis deviation from the normal to the film surface is 9 and 11 degrees.

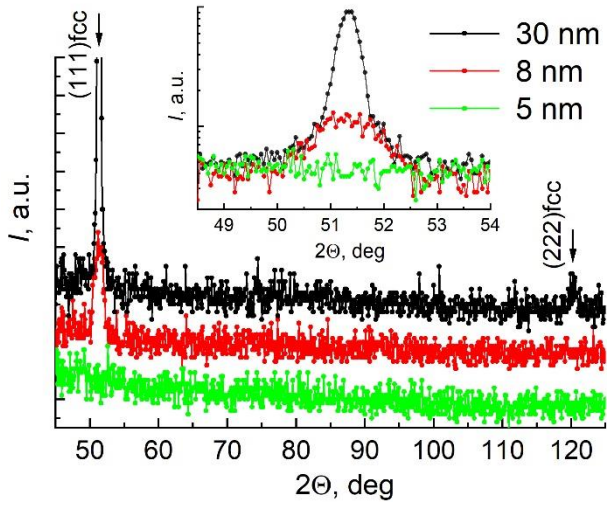

Figure 2: X-ray diffraction results for NiFeCr films with 5, 8 and 30 nm thickness. The inset shows the (111) fcc reflection, obtained by measuring in a smaller angular range and at longer exposure time.

The images obtained using AFM microscopy (Fig.3) show that the surface of 5nm thick films looks different from the surface of thicker films t_{NiFeCr} = 8 and 30 nm.

The difference is in the finer dispersion and a larger number of pores. The observed surface morphology comes to agreement with the conclusions, made according to the X-ray investigation results, about the X-ray amorphous disordered microstructure and lower density of the material

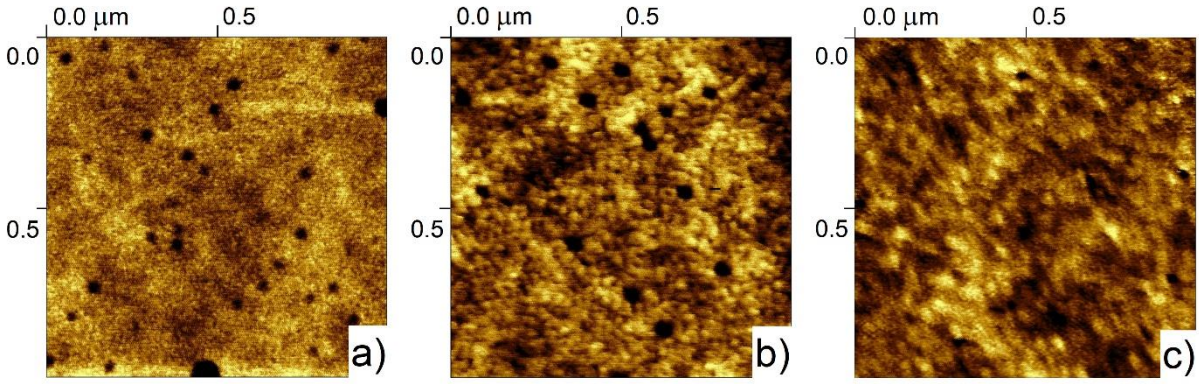

Figure 3: Images of the surface of films with thickness of 5 nm (a), 8 nm (b) and 30 nm (c), obtained by AFM microscopy.

Crystal grains with the average lateral size of approximately 30 nm are seen on the surface of t_{NiFeCr} = 8 nm thick sample, which has polycrystalline fcc structure and the most perfect <111> texture. With the increase of film thickness to t_{NiFeCr} = 30 nm the size of crystallites increases. The surface roughness, estimated as the root-mean-square deviation (rms) and measured on the area of 1mkm × 1 mkm, is rms = 0.24, 0.22 and 30 nm. The obtained rms values are very close to each other, what comes in agreement with the results of X-ray reflectometry.

Thus, the microstructure and morphology of film surface at t_{NiFeCr} = 5 nm differs significantly from that, obtained for t_{NiFeCr} = 8 and 30 nm. In particular, at t_{NiFeCr} = 8 and 30 nm the polycrystalline films have fcc structure and axial texture <111>, while at t_{NiFeCr} = 5 nm the X-ray amorphous film has a disordered microstructure, small grain size, larger number of pores and lower material density and electron density, as compared to the t_{NiFeCr} = 8 and 30 nm samples.

Specific electrical resistance and temperature coefficient of resistance for $Ni_{48}Fe_{12}Cr_{40}$ films

Fig. 4 shows the temperature dependences of electrical resistance and temperature coefficient of resistance (TCR) of $Ni_{48}Fe_{12}Cr_{40}$ films with thickness of 5 and 8 nm. The specific resistance of the studied $Ni_{48}Fe_{12}Cr_{40}$ films exceeds significantly the values common to polycrystalline $Ni_{48}Fe_{12}Cr_{40}$ films (20-30 μOhm·cm). The growth in the electrical resistance, due to the heavy alloying – introduction of high concentration of Cr, leads to the significant increase of impurity electron scattering. Additional contribution is made by the size effect, associated with the scattering of charge carriers on the thin film surfaces.

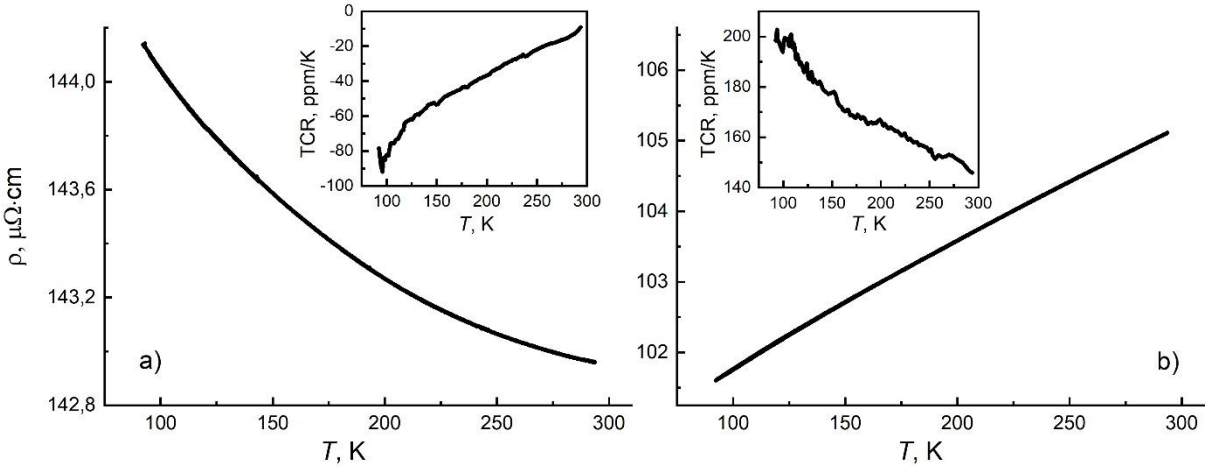

Figure 4: Temperature dependencies of specific electrical resistance and temperature coefficient of resistance for $Ni_{48}Fe_{12}Cr_{40}$ films with thickness of 5 nm (a) and 8 nm (b).

For the $Ni_{48}Fe_{12}Cr_{40}$(5nm) film a negative TCR was observed, the decrease of temperature was accompanied by the increase in specific electrical resistance. This situation is typical for the highly disordered systems and is caused by the strong scattering of charge carriers due to the small length of free path [11]. With the increase in $Ni_{48}Fe_{12}Cr_{40}$ film thickness from 5 to 8 nm, the change in TCR sign from negative to positive was observed and the temperature dependence of specific electrical resistance of the $Ni_{48}Fe_{12}Cr_{40}$(8nm) film took the typical of metals form: a decrease in

temperature was accompanied by a decrease in the value of specific electrical resistance. The increase in $Ni_{48}Fe_{12}Cr_{40}$ film thickness also led to the increase in the absolute value of TCR, caused by the increase of grain size. The increase in the absolute value of TCR observed at the decrease in temperature for $Ni_{48}Fe_{12}Cr_{40}$ films of 5 and 8 nm thick is apparently associated with the increase in the length of free path of charge carriers due to the decrease in the contribution of phonon scattering.

Magnetoresistance of $Ni_{48}Fe_{12}Cr_{40}$ thin films

Fig. 5 shows the field dependencies of magnetoresistance for the $Ni_{48}Fe_{12}Cr_{40}$(5nm) film, measured at different temperatures and external magnetic field orientations.

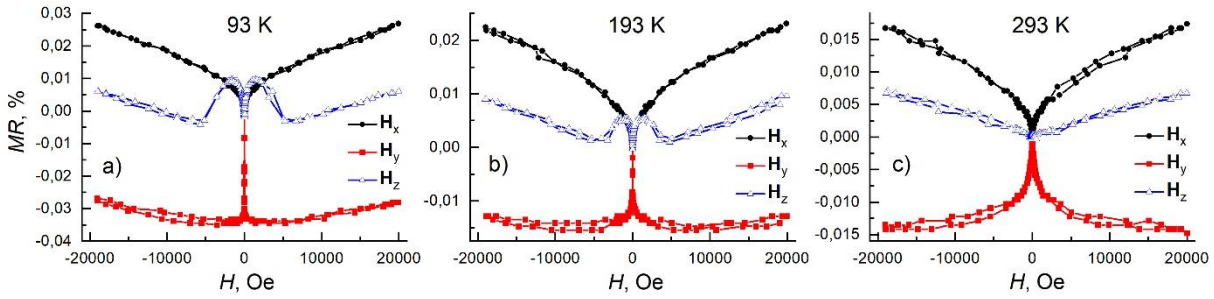

Figure 5: Field dependencies of magnetoresistance for $Ni_{48}Fe_{12}Cr_{40}$(5nm) at different orientations of external magnetic field at temperatures 93K (a), 193K (b) and 293K (c).

Possible explanation of the observed magnetoresistance is the existence of ferromagnetic ordering in the $Ni_{48}Fe_{12}Cr_{40}$(5nm) film. Anisotropic magnetoresistance is maximum in case of collinear orientation of the ferromagnet magnetic moment and electric current flowing through the sample, and minimum at orthogonal orientation. It is reported in [4], that NiFeCr alloys can have ferromagnetic ordering, and the Curie temperature depends on the Cr concentration introduced into NiFe composition and on the film thickness.

Let us analyze the nature of the field dependencies of magnetoresistance for $Ni_{48}Fe_{12}Cr_{40}$(5nm) film at different orientations of external magnetic field.

Longitudinal magnetoresistance MR_x in $\mathbf{H}_x$ field:

Longitudinal magnetoresistance is positive in the temperature range of 93 – 293 K and is caused by the external magnetic field that aligns the magnetic moments in the film along the electric current. With the increase of temperature, the value of MR_x decreases from 0.026 to 0.016% due to the weakening of magnetic ordering.

Transverse magnetoresistance MR_y in $\mathbf{H}_y$ field:

On the dependence $MR_y(H)$ two sections can be seen: 1) in the range of low fields a sharp drop of magnetoresistance occurs; and 2) with further increase in the magnetic field a sharp drop of magnetoresistance is observed and the slope of $MR_y(H)$ dependence depends on the temperature.

In $\mathbf{H}_y$ field magnetic moments are ordered orthogonally to the electric current. This causes a sharp decrease of magnetoresistance MR_y in the low fields. The value of magnetoresistance decreases with the increase of temperature, what is typical for AMR, since the magnetic moment decreases and the contribution of phonon scattering increases. It is interesting to see that at T = 293 K the MR_y value continues to decrease with the increase of magnetic field. This may be due to the reorientation of those magnetic moments that have not yet been ordered. With the decrease of temperature this tendency changes, and the growth of magnetoresistance is observed at the increase of magnetic field. The contribution of magnetoresistance (OMR) caused by the Lorentz force, effecting on charge carriers, becomes noticeable [18].

Orthogonal magnetoresistance MR_z in $\mathbf{H}_z$ field:

In the field range of ±5 kOe there are features, on the field dependencies MR_z at T = 93 K, that become less noticeable with the temperature increase and disappear at T = 293 K. The further increase in the magnetic field is accompanied by the increase of magnetoresistance value.

The observed features on $MR_z(H)$ dependence in the field range of ±5 kOe at T = 93 K can occur due to the exit of magnetic moment from the film plane. In the fields up to ±1.5 kOe the growth of MR_z value is observed. A possible reason is the non-strictly orthogonal orientation of $\mathbf{H}_z$ field relative to the film plane. The appearance of non-zero field projection in the film plane can lead to the ordering of magnetic moments collinearly to the electric current, what is accompanied by the increase of magnetoresistance (AMR) effect. At further increase of the magnetic field (up to ±5 kOe), the magnetoresistance value decreases, what is caused by the magnetic moment exit from the film plane and formation of the orthogonal configuration of magnetization and electric current. The saturation field (~5kOe) in this case, corresponds to the demagnetizing field $H_{sat} = 4\pi M_S$. The further increase of the magnetic field is accompanied by the linear growth of MR_z, what is due to the OMR contribution.

With the temperature increase to 293 K the peculiar features of magnetoresistance in low fields disappear, what can be the consequence of decrease in saturation magnetization due to the vicinity of alloy to ferromagnetic – paramagnetic phase transition.

According to studies [19], the segregation of chromium atoms on the boundaries of nanoparticles is observed for Ni-Cr alloys. In conditions of thin film, it can lead to the formation of ferromagnetic clusters with low Cr content, separated by Cr-rich boundaries. It is probable, that in the 5 nm thick film under investigation, the observed AMR (and the presence of long-range ferromagnetic order) is also due to the chemical inhomogeneity and clustering of Ni and Fe atoms.

With the increase of $Ni_{48}Fe_{12}Cr_{40}$ film thickness from 5 to 8 nm, a change in the shape of field dependence of magnetoresistance and decrease of the effect value are observed (Fig. 6). The possible reason is the evolution of film microstructure.

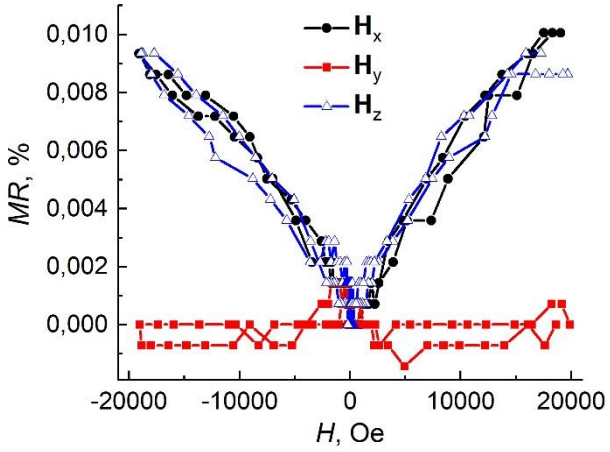

Figure 6: Field dependencies of magnetoresistance for $Ni_{48}Fe_{12}Cr_{40}$(8nm) film at different orientations of external magnetic field at temperature 93K.

A peculiar feature of the field dependencies of magnetoresistance of $Ni_{48}Fe_{12}Cr_{40}$(8nm) film is almost a complete coincidence of the curves for longitudinal ($\mathbf{H}_x$) and orthogonal ($\mathbf{H}_z$) orientations of the magnetic field, $MR_x(H)$ and $MR_z(H)$ demonstrate the linear positive growth with increasing H. As shown in the work [20], the positive, linear in the field and isotropic magnetoresistance is a characteristic feature of thin films of granular ferromagnetic metals (Ni, Fe, Co). The dominant mechanism in such systems is the ordinary magnetoresistance (OMR), caused by the Lorentz force and the effects of paths curvature of the current flow in conditions of inhomogeneous medium [21].

The transverse magnetoresistance of the film (in $\mathbf{H}_y$ field) does not depend practically on the magnetic field strength. The reason may be in the mutual compensation of two contributions: negative AMR and positive OMR. However, unlike the orthogonal geometry ($\mathbf{H}_z$), the OMR contribution is significantly weakened by the size effect and charge carriers scattering on the thin film surfaces.

With the temperature increase to 293 K the nature of field dependencies of magnetoresistance is preserved, and the magnitude of effect decreases by ~1.5 times, what is associated with the increase of phonon scattering.

Unlike the 5 nm thick film, the $Ni_{48}Fe_{12}Cr_{40}$(8nm) film does not exhibit a pronounced AMR. According to the microstructure investigation data, the increase of film thickness is accompanied by the crystallization and texture formation. This process, probably, contributes to the more uniform distribution of Cr atoms in Ni-Fe matrix and to the effective suppression of magnetic moments.

It is important to note, that the geometry, where the magnetoresistance for $Ni_{48}Fe_{12}Cr_{40}$ film of 8nm thickness is observed, coincides with the configuration required for observation of Hanle magnetoresistance [22]. In this connection, the mechanism of suppression of spin accumulation can be considered as an alternative interpretation of the observed phenomena. To determine the dominant mechanism for certain, the additional studies are necessary.

Hall effects in $Ni_{48}Fe_{12}Cr_{40}$ thin films

Figure 7 shows the field dependencies of the Hall resistance for $Ni_{48}Fe_{12}Cr_{40}$ films with thickness of 5 and 8 nm.

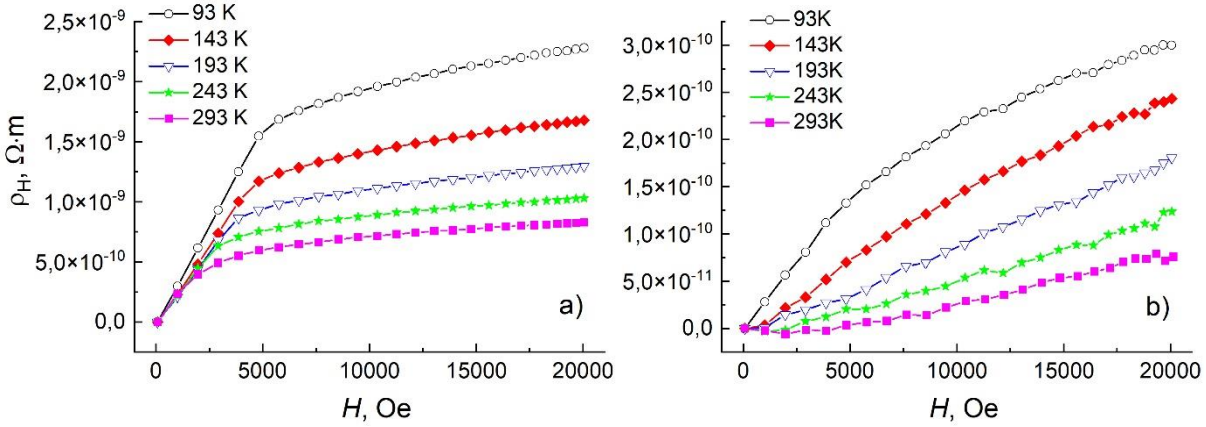

Figure 7: Dependencies $\rho_H(H)$ for $Ni_{48}Fe_{12}Cr_{40}$ films with thickness of 5 nm (a) and 8 nm (b).

Dependencies $\rho_H(H)$ for $Ni_{48}Fe_{12}Cr_{40}$(5nm) film demonstrate the behavior characteristic of ferromagnetic materials with dominant contribution from anomalous Hall effect [23-25]. In the region of low fields (<5 kOe for T = 93 K) a linear increase in

the signal is observed, associated with the process of aligning the magnetic moments orthogonally to the film plane. Upon reaching the saturation (~5 kOe, T = 93K) a bend is observed on the dependence, followed by more graduate increase of ρ_H with increasing magnetic field. It is important to note, that the saturation field determined from the bend point of $\rho_H(H)$ dependence at T = 93 K, coincides quantitatively with the saturation field of magnetoresistance in orthogonal geometry of magnetic field ($\mathbf{H}_z$) at T = 93 K (Fig. 5a). This correlation confirms, that both galvanomagnetic effects (anisotropic magnetoresistance and anomalous Hall effect) are associated with the magnetic moments exit from the plane at the increase of H_z.

Analysis of $\rho_H(H)$ dependencies shows, that the bend point corresponding to the saturation field shifts to the lower field area at the increase of temperature. The magnitude of this field makes it possible to estimate the saturation magnetization of material ($H_{sat} = 4\pi M_S$). As a result, for $Ni_{48}Fe_{12}Cr_{40}$(5nm) film the value of M_S decreases from 430 to 200 emu/cm^3 with the growth of temperature from 93 to 293 K. For comparison, the saturation magnetization of $Ni_{80}Fe_{20}$ permalloy films is on the order of 800 emu/cm³ and is practically constant in the specified temperature range due to the distance from Curie temperature (~850K) [26-28]. Significant decrease in magnetization in $Ni_{48}Fe_{12}Cr_{40}$(5nm) is due to the dilution of the magnetic subsystem with chromium atoms. Moreover, the pronounced temperature dependence of M_S indicates the sharp decrease in Curie temperature of the alloy compared to permalloy and is a sign of system proximity to the magnetic phase transition.

For the $Ni_{48}Fe_{12}Cr_{40}$(8nm) film the character of dependencies changes approaching the linear form, which is typical of nonmagnetic metals (Figure 7b). At low temperatures (93, 143K), a weak nonlinearity of signal is still visible in the curves. The presence of residual contribution from the anomalous Hall effect indicates the preservation of ferromagnetic ordering in the film in this temperature range, however,

the amplitude of this contribution is smaller by an order of magnitude than in the $Ni_{48}Fe_{12}Cr_{40}$(5nm) film. With a further increase in temperature (193-293K), the field dependencies of the Hall resistance become linear.

The decrease of slope of $\rho_H(H)$ dependencies with increasing temperature is an important peculiarity. As a rule, for nonmagnetic metals the slope of $\rho_H(H)$ (and Hall coefficient, respectively) does not depend on temperature [29]. In this case, the observed temperature dependence of the slope indicates, that the measured signal has the contribution related to magnetism. Apparently, despite a more uniform distribution of Cr atoms in the matrix compared to $Ni_{48}Fe_{12}Cr_{40}$(5nm) film, the magnetic ordering in the local clusters is preserved; however, their collective response to the external magnetic field weakens due to the growth of thermal fluctuations.

It should be noted separately, that for the studied $Ni_{48}Fe_{12}Cr_{40}$ films of 5 and 8 nm in thickness the slope coefficient of $\rho_H(H)$ dependencies (and hence the Hall constant R_0) has a positive sign. This result is in agreement with the data for pure Cr [30, 31] and disordered Ni-based alloys [2, 29], which are specified by the hole type of conductivity. Quantitative estimation of the Hall coefficients showed that for 5 and 8 nm films the Hall constant R_0 varies within the range of $1.2\text{-}3.6\cdot10^{-10}$ m^3/C and $5.5\text{-}8.4\cdot10^{-11}$ m^3/C, respectively, in the temperature range of 93 - 293 K. At that, the coefficient of anomalous Hall effect R_S for 5 nm film reaches the values of $2.4\text{-}2.9\cdot10^{-9}$ m^3/C.

The obtained experimental data are in good qualitative and quantitative agreement with the results of the work [13], where the positive signs of the coefficients $R_0 = 4.2\cdot10^{-11}$ m^3/C and $R_S = 2.3\cdot10^{-9}$ m^3/C were also observed for the massive $Ni_{73.5}Fe_8Cr_{18.5}$ alloy. The authors conclude that in this alloy the dominant mechanism of the anomalous Hall effect is a lateral displacement (side-jump), which prevails in the systems with strong scattering, namely with high specific resistance and small length

of free path. Taking into account the good correlation of R_S estimation for $Ni_{48}Fe_{12}Cr_{40}$(5nm) with the data of [13], it can be assumed that transport properties of the investigated films are determined by the same scattering mechanisms as in the massive NiFeCr alloys.

The results of measuring the planar Hall effect (PHE), which is connected with anisotropic magnetoresistance in ferromagnets, confirm the conclusions about the magnetic ordering of the investigated films. Fig. 8 shows the angular dependencies of PHE amplitude in the external field of H = 20 kOe, applied in the plane for 5 and 8 nm films at T = 93 K. The experimental data are successfully approximated by the periodic function sin(2α), and the extrema are observed at α = -45°, 135° (maximum) and α = 45°, 225° (minimum), what is typical of the planar Hall effect [32].

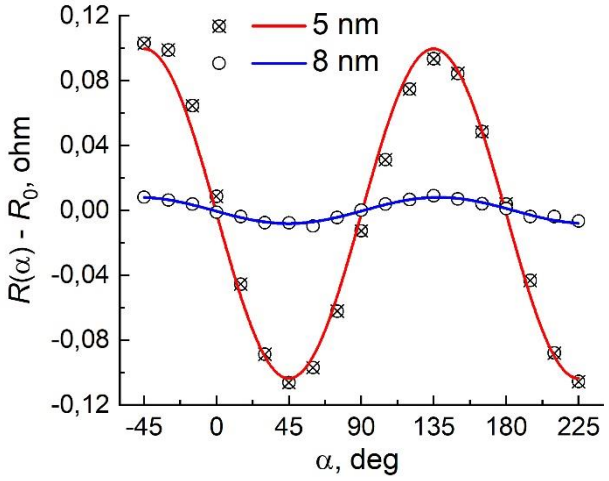

Figure 8: Angular dependence of planar Hall effect amplitude in the field H = 20 kOe for $Ni_{48}Fe_{12}Cr_{40}$ films of 5 and 8 nm thickness at T = 93 K. α is the angle between the electric current direction and the external magnetic field, the symbols indicate the experimental data, the lines are the result of approximation.

The $Ni_{48}Fe_{12}Cr_{40}$(5nm) film exhibits the pronounced amplitude of PHE, which together with the presence of anomalous contribution to the Hall effect and the observation of anisotropic magnetoresistance, confirms the assumption of ferromagnetic ordering of the sample. The PHE amplitude for $Ni_{48}Fe_{12}Cr_{40}$(8nm) is by

the order of magnitude lower, what indicates the suppression of ferromagnetic ordering. Moreover, the presence of weak but noticeable PHE signal, the nonlinearity of Hall curves at low temperatures and the dependence of their slope on the temperature can be a mark of existence of the local magnetic clusters.

Conclusion

Complex studies of microstructure, as well as the transport and galvanomagnetic properties of $Ni_{48}Fe_{12}Cr_{40}$ thin films synthesized by magnetron sputtering on glass substrates allow us to draw the following conclusions:

The 5 nm film thick is X-ray amorphous and has a disordered fine-crystalline microstructure. The 8- and 30-nm-thick films are polycrystalline. As the film thickness increases, a face-centered cubic structure and <111> axial texture is formed, along with the increase of grain size and material density. All the studied films have similar values of surface roughness.

The correlation between microstructure and transport properties is revealed. The negative temperature coefficient of resistance is observed for amorphous film of 5 nm thickness due to the strong scattering of charge carriers in the disordered systems. The increase of film thickness leads to the sign inversion of temperature coefficient of resistance and increase in its absolute value, what is connected with the increase of grain size.

The observation of anisotropic magnetoresistance, anomalous contribution to the Hall effect and pronounced amplitude of the planar Hall effect for 5 nm thick film allow us to make a conclusion that this sample has a ferromagnetic ordering.

The saturation magnetization of the 5nm thick film decreases from 430 to 200 emu/cm^3 with the increasing temperature from 93 to 293 K, which is by 2-4 times lower

than the characteristic values of pure permalloy. The sharp temperature dependence of saturation magnetization indicates the significant decrease of Curie temperature of the alloy compared to the permalloy and is the evidence of system closeness to magnetic phase transition.

The increase of the film thickness from 5 to 8 nm leads to the more uniform distribution of Cr atoms in Ni-Fe matrix and suppression of the long-range ferromagnetic order. However, the peculiarities of field dependencies of Hall resistance and the presence of planar Hall effect for the 8 nm thick film indicate the existence of local magnetic clusters.

Experimental

$Ni_{48}Fe_{12}Cr_{40}$ films with thickness of t_{NiFeCr} = 5, 8 and 30 nm were fabricated by magnetron sputtering (high vacuum precision magnetron setup MPS-4000-C6 (ULVAC Inc., Japan)) on glass substrates. Sputtering was carried out at room temperature and 100 W power on the $Ni_{48}Fe_{12}Cr_{40}$ alloy target. The target was purchased from Girmet Ltd (Russia). The pressure of working gas (argon, 99.999% purity) in the sputtering chamber was 0.1 Pa with the residual gas base pressure of $5 \cdot 10^{-7}$ Pa.

To study the galvanomagnetic properties of $Ni_{48}Fe_{12}Cr_{40}$ thin films, Hall bridge-shaped micro-objects (Fig.9) were patterned using a SUSS MicroTec MJB4 optical photolithography system (Germany). The current channel width was w = 200 μm, and the distance between current (1,2) and potential (3,4) contact pads were 2700 μm and 2200 μm, respectively. The electrical resistance of the micro-objects was measured in the temperature range of 93 – 293 K using the setup based on electromagnet, the pumping cryostat and temperature controller.

When measuring the magnetoresistance, the external magnetic field was applied collinearly ($\mathbf{H}_x$) and orthogonally ($\mathbf{H}_y$) to the direction of the electric current in the film plane, as well as orthogonally to the direction of the electric current and the film plane ($\mathbf{H}_z$). Magnetoresistance was determined as $MR(H) = (R(H)-R(0))/R(0)\times100\%$, where $R(H)$ is the electrical resistance in the field H, $R(0)$ is the electrical resistance in the field $H = 0$. The magnitude of the applied field varied in the range of ±20 kOe.

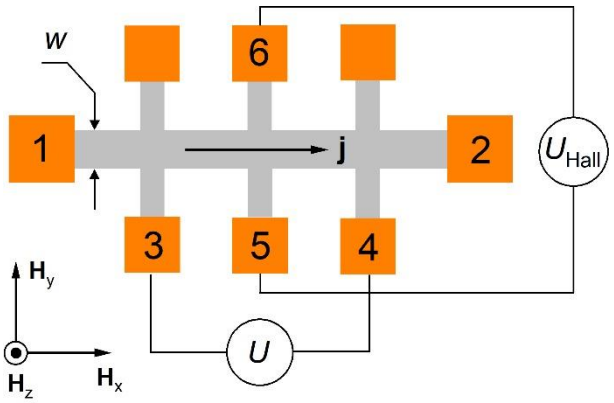

Figure 9: Schematic image of the Hall bridge.

When studying the Hall effect, the external magnetic field was directed orthogonally to the sample plane ($\mathbf{H}_z$) and varied within the range of ±20 kOe. The magnitude of electric current flowing through the microstrip during the measurements was 1 mA. Field dependencies of the Hall resistance were obtained in the temperature range of 93 – 293 K. To minimize the contribution of contact asymmetry (5,6), the measured Hall voltage values were averaged for the opposite directions of magnetic field and current.

When studying the planar Hall effect, the magnetic field was directed in the film plane. The angle between the magnetic field and direction of electric current (α) was varied in the range of -45 – 225°. The amplitude of planar Hall effect was determined as $R(\alpha) - R_0$, where $R(\alpha)$ and R_0 are the transverse resistance of the sample in positions α and α=0°, respectively.

The microstructure of the thin films was investigated using a DRON-3M automated X-ray diffractometer (Russia) in Co Kα radiation. Surface topography was investigated using a Solver Next atomic force microscope (NT-MDT, Russia) operating in semi-contact mode. Measurements were performed under ambient conditions (20°C, ~25% relative humidity) using HA-NC silicon cantilevers with a tip radius < 10 nm, a resonance frequency of 235 kHz, and a force constant of 12 N/m. Scans of 1 × 1 μm^2 areas were acquired at a 1 Hz rate with a 5–10 nm step. The obtained images were analyzed using Nova and Gwyddion 2.55 software.

Funding

The work was carried out within the framework of the state assignment of the Ministry of Science and Higher Education of the Russian Federation for the IMP UB RAS

Author Contributions

Roman Zavornitsyn – Investigation, Data curation, Visualization, Writing – original draft

Mikhail Milyaev – Resources, Funding acquisition

Larisa Naumova – Investigation, Validation, Writing – review and editing

Irina Maksimova – Methodology

Anastasia Pavlova – Methodology

Tatyana Chernyshova – Methodology

Vyacheslav Proglyado – Methodology

Vladimir Ustinov – Conceptualization, Project administration

References

1. Ritzinger, P.; Výborný, K. R. Soc. Open Sci., 2023, 10, 230564. doi: 10.1098/rsos.230564

2. McGuire, T. R.; Potter, R. I. IEEE Trans. Magn., 1975, 11, 1018–1038. doi: 10.1109/TMAG.1975.1058782

3. Willard, J.; Mishra, S. S.; Klaes, R. M.; Emtage, N. J.; Loloee, R.; Birge, N. O. J. Appl. Phys., 2025, 137, 123909. doi: 10.1063/5.0257749

4. Devonport, A.; Vishina, A.; Singh, R. K.; Edwards, M.; Zheng, K.; Domenico, J.; Rizzo, N. D.; Kopas, C.; van Schilfgaarde, M.; Newman, N. J. Magn. Magn. Mater., 2018, 460, 193–202. doi: 10.1016/j.jmmm.2018.03.054

5. Lee, W. Y.; Toney, M. F.; Mauri, D. IEEE Trans. Magn., 2000, 36, 381–385. doi: 10.1109/20.822551

6. Yen, Y.-W.; Su, J.-W.; Huang, D.-P. J. Alloys Compd., 2008, 457, 270–278. doi: 10.1016/j.jallcom.2007.03.053

7. Bannikova, N. S.; Milyaev, M. A.; Naumova, L. I.; Krinitsina, T. P.; Patrakov, E. I.; Proglyado, V. V.; Chernyshova, T. A.; Ustinov, V. V. Phys. Solid State, 2016, 58, 2011–2017. doi: 10.1134/S1063783416100061

8. Fassbender, J.; von Borany, J.; Mücklich, A.; Potzger, K.; Möller, W.; McCord, J.; Schultz, L.; Mattheis, R. Phys. Rev. B, 2006, 73, 184410. doi: 10.1103/PhysRevB.73.184410

9. Phuong, N. M.; Kim, D.-J.; Kang, B.-D.; Kim, C. S.; Yoon, S.-G. J. Electrochem. Soc., 2006, 153, G27. doi: 10.1149/1.2129332

10. Vinayak, S.; Vyas, H. P.; Vankar, V. D. Thin Solid Films, 2007, 515, 7109–7116. doi: 10.1016/j.tsf.2007.03.012

11. Mooij, J. H. Phys. Status Solidi A, 1973, 17, 521–530.
doi: 10.1002/pssa.2210170217
12. Pal, P.; Majumdar, A. K.; Nigam, A. K. J. Magn. Magn. Mater., 2015, 381, 297–309. doi: 10.1016/j.jmmm.2015.01.006
13. Chakraborty, S.; Majumdar, A. K. Phys. Rev. B, 1998, 57, 11850–11852.
doi: 10.1103/PhysRevB.57.11850
14. Wu, P.; Gao, Y.; Qiu, H.; Pan, L.; Tian, Y.; Wang, F. Rare Metals, 2007, 26, 176–181. doi: 10.1016/S1001-0521(07)60180-6
15. Talantsev, A.; Elzwawy, A.; Kim, C. J. Appl. Phys., 2018, 123, 173902.
doi: 10.1063/1.5023888
16. Petrakov, A. P. Tech. Phys., 2003, 48, 508–513. doi: 10.1134/1.1568495
17. Yasaka, M. The Rigaku Journal, 2010, 26, 1–9.
18. McGuire, T. R. AIP Conf. Proc., 1975, 24, 435–436. doi: 10.1063/1.29940
19. Bohra, M.; Grammatikopoulos, P.; Diaz, R. E.; Singh, V.; Zhao, J.; Bobo, J.-F.; Kuronen, A.; Djurabekova, F.; Nordlund, K.; Sowwan, M. Chem. Mater., 2017, 29, 4361–4369. doi: 10.1021/acs.chemmater.5b00837
20. Gerber, A.; Kishon, I.; Korenblit, I. Ya.; Riss, O.; Segal, A.; Karpovski, M.; Raquet, B. Phys. Rev. Lett., 2007, 99, 027201. doi: 10.1103/PhysRevLett.99.027201
21. Parish, M. M.; Littlewood, P. B. Phys. Rev. B, 2005, 72, 094417.
doi: 10.1103/PhysRevB.72.094417
22. Vélez, S.; Golovach, V. N.; Bedoya-Pinto, A.; Isasa, M.; Sagasta, E.; Abadia, M.; Rogero, C.; Hueso, L. E.; Bergeret, F. S.; Casanova, F. Phys. Rev. Lett., 2016, 116, 016603. doi: 10.1103/PhysRevLett.116.016603
23. Nagaosa, N.; Sinova, J.; Onoda, S.; MacDonald, A. H.; Ong, N. P. Rev. Mod. Phys., 2010, 82, 1539–1592. doi: 10.1103/RevModPhys.82.1539

24. Pugh, E. M.; Rostoker, N. Rev. Mod. Phys., 1953, 25, 151–157. doi: 10.1103/RevModPhys.25.151

25. Schad, R.; Beliën, P.; Verbanck, G.; Moshchalkov, V. V.; Bruynseraede, Y. J. Phys.: Condens. Matter., 1998, 10, 6643. doi: 10.1088/0953-8984/10/30/005

26. O'Handley, R. C. Modern Magnetic Materials: Principles and Applications, Wiley-Interscience, 2000, 83–86.

27. Ingvarsson, S.; Xiao, G.; Parkin, S. S. P.; Koch, R. H. Appl. Phys. Lett., 2004, 85, 4995–4997. doi: 10.1063/1.1828232

28. Freedman, J. F.; Mayadas, A. F.; Klokholm, E. IEEE Trans. Magn., 1969, 5, 170–176. doi: 10.1109/TMAG.1969.1066466

29. Hurd, C. M. The Hall Effect in Metals and Alloys, Plenum Press, 1972.

30. Fawcett, E. Rev. Mod. Phys., 1988, 60, 209. doi: 10.1103/RevModPhys.60.209

31. Foner, S. Phys. Rev., 1957, 107, 1513–1516. doi: 10.1103/PhysRev.107.1513

32. Yu, M. L.; Chang, J. T. H. J. Phys. Chem. Solids, 1970, 31, 1997–2002. doi: 10.1016/0022-3697(70)90003-X